Science
AAAS

High-Frequency, Long-Range Coupling Between Prefrontal and Visual Cortex During Attention

Georgia G. Gregoriou, *et al.*

Science **324**, 1207 (2009);
DOI: 10.1126/science.1171402

Science (print ISSN 0036-8075; online ISSN 1095-9203) is published weekly, except the last week in December, by the American Association for the Advancement of Science, 1200 New York Avenue NW, Washington, DC 20005.

High-Frequency, Long-Range Coupling Between Prefrontal and Visual Cortex During Attention

Georgia G. Gregoriou,[1]* Stephen J. Gotts,[2]* Huihui Zhou,[1] Robert Desimone[1]†

Electrical recordings in humans and monkeys show attentional enhancement of evoked responses and gamma synchrony in ventral stream cortical areas. Does this synchrony result from intrinsic activity in visual cortex or from inputs from other structures? Using paired recordings in the frontal eye field (FEF) and area V4, we found that attention to a stimulus in their joint receptive field leads to enhanced oscillatory coupling between the two areas, particularly at gamma frequencies. This coupling appeared to be initiated by FEF and was time-shifted by about 8 to 13 milliseconds across a range of frequencies. Considering the expected conduction and synaptic delays between the areas, this time-shifted coupling at gamma frequencies may optimize the postsynaptic impact of spikes from one area upon the other, improving cross-area communication with attention.

A typical crowded scene contains many objects that cannot be processed simultaneously, thus requiring attentional mechanisms to select the ones most relevant to behavior. Electrophysiological studies in monkeys have shown that attention leads to enhanced responses of neurons in ventral stream areas that are important for object recognition, at the expense of responses to distracting stimuli (*1*). Moreover, attention increases neural synchrony, often in the gamma frequency range (*2*–*5*). Given that cells have limited integration times, increases in synchrony and firing rates may together have a larger impact on downstream neurons and thus increase the effectiveness of behaviorally relevant stimuli (*6*, *7*). Areas in the prefrontal cortex (PFC) and parietal cortex may be sources of the top-down attentional feedback to ventral stream areas, which could enhance firing rates with attention (*1*, *4*, *8*). However, the mechanisms that cause increases in neural synchrony with attention in visual cortex are unknown.

We investigated whether the frontal eye field (FEF), an area within the PFC, is a source of enhanced neural synchrony effects in area V4 during attention. The FEF has reciprocal connections with V4 (*9*–*11*), and electrical stimulation of FEF enhances V4 neuronal responses to a stimulus in the receptive field (RF) (*12*, *13*). We recorded spikes (multi-unit) and local field potentials (LFPs) simultaneously from FEF and V4 in two monkeys trained in a covert attention task (Fig. 1A) (*14*). One grating stimulus appeared inside the shared RF, and two others appeared outside. After a variable delay, the spot at fixation changed color (which was the cue) so as to match the color of one of the three gratings, indicating the target stimulus to be attended. The monkey was rewarded for releasing a bar when the target stimulus changed color.

We first verified that attention caused enhanced firing rates in FEF and V4. We recorded from 292 sites with visual responses in FEF and 262 sites in V4. The results were qualitatively similar (and statistically significant) in both monkeys and were therefore combined. Figure 1, B and C, shows the average normalized response of the population of FEF and V4 neurons, respectively, for conditions with overlapping RFs. Neuronal responses were significantly increased by attention to the joint RF in both areas (average response in a window 100 to 800 ms after cue onset; Wilcoxon sign-rank test, $P < 0.001$) and remained significantly enhanced until the end of the trial (average response in a window 500 ms before the target's color change; Wilcoxon sign-rank test, $P < 0.001$) [for the distribution of attentional effects on firing rate, see the supporting online material (SOM) text].

Attentional effects on firing rates occurred significantly earlier in FEF than in V4 (at 80 ms after the cue in FEF, and 130 ms after the cue in V4) [Fig. 1, B and C dashed lines; $P = 0.017$ two-sided permutation test (SOM text)]. The distribution of attentional latencies is shown separately for FEF and V4 in Fig. 1, D and E, and was similarly shifted earlier for FEF (Wilcoxon rank-sum test, $P < 0.001$) (for a table of latency measurements, see table S1).

We next used multi-taper spectral methods to calculate the coherence between spikes and LFPs (*14*). Spike-field coherence in the gamma band significantly increased with attention within each area (coherence averaged between 40 and 60 Hz; paired t test, $P < 0.001$ in both areas), whereas low frequencies were desynchronized (average coherence between 5 and 20 Hz; paired t test, $P < 0.001$ in both areas) (Fig. 2, A and B). At the population level, gamma band coherence increased by 14% in V4 (*2*, *3*, *15*) and by 22% in the FEF (for distributions of effects, see SOM text).

If FEF is the source of enhanced synchrony in V4, the critical question is whether attention

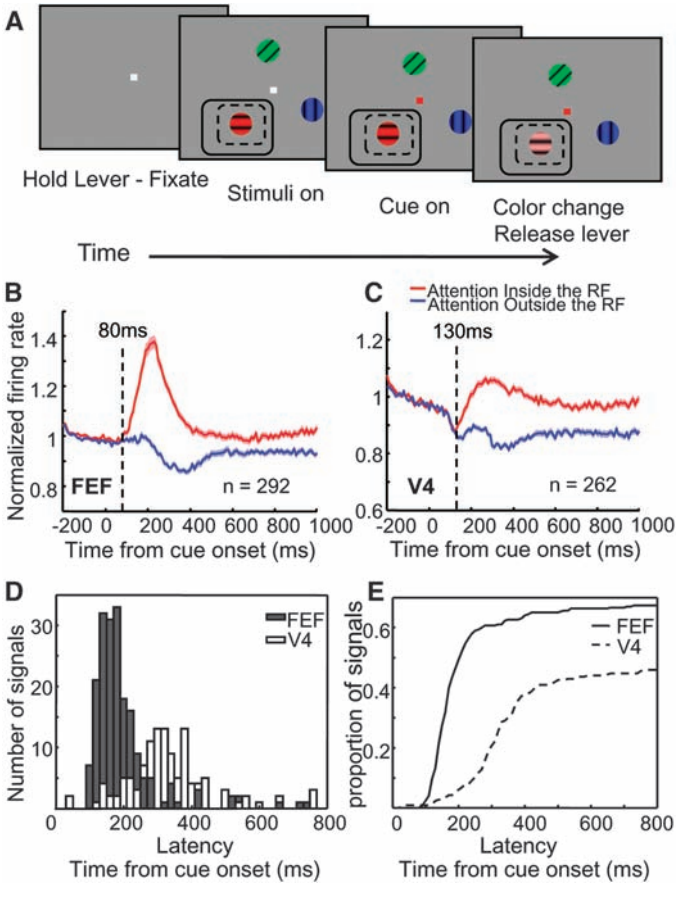

Fig. 1. (**A**) Illustration of behavioral task. Dashed- and solid-line rectangles indicate hypothetical overlapping RFs for V4 and FEF sites, respectively. (**B** and **C**) Normalized firing rates averaged across the population of cells in FEF and V4, respectively. SEM (±) at each time point is indicated by shading over the lines. Vertical dashed lines indicate latency of attentional effects at the population level. (**D**) Distribution of attentional latencies in the firing rates of FEF and V4 neurons. (**E**) Cumulative distribution of FEF and V4 latencies, represented as a proportion of recordings in which latencies could be reliably estimated.

[1]McGovern Institute for Brain Research, Massachusetts Institute of Technology, Cambridge, MA 02139, USA. [2]Laboratory of Brain and Cognition, National Institute of Mental Health, National Institutes of Health, Bethesda, MD 20892, USA.

*These authors contributed equally to this work.
†To whom correspondence should be addressed. E-mail: desimone@mit.edu

increases coupled oscillations between the two areas. We found that the attentional effect on gamma frequency spike-field coherence between areas was even larger than the effects within areas (Fig. 2, C and D). With attention, gamma coherence between V4 spikes and FEF LFPs increased by 26% at the population level (paired *t* test, $P < 0.001$), between FEF spikes and V4 LFPs increased by 37% (paired *t* test, $P < 0.001$), and remained enhanced through the end of the trial (paired *t* test, $P < 0.001$ for all pair types). All of these effects were highly dependent on RF overlap at the locus of attention. For pairs of recordings with nonoverlapping RFs, coherence in the two attention conditions did not differ from that in the pre-stimulus period (one-way analysis of variance, $P = 0.86$) (Fig. 2F and SOM text).

Gamma frequency coherence between LFPs recorded across the two areas was enhanced 63% by attention (Fig. 2E) (paired *t* test, $P < 0.001$), and gamma coherence between spike trains across areas was enhanced by 13% (paired *t* test, $P < 0.001$). In general, spike-spike coherence across electrodes is smaller than spike-field and field-field coherence for statistical reasons (*16*). Another probable factor is that connections between FEF and V4 are patchy (*9*, *10*), and LFPs sum signals over a wider area.

We considered whether the synchronous oscillations between V4 and FEF might have resulted from a common oscillatory input, which would be expected to result in zero phase-lag synchrony between the areas. To test for this, we computed the distribution of the coherence phase shifts within and across areas. Within areas, the distribution of the average (between 40 and 60 Hz) relative phase between the two recorded signals (Fig. 3) had a median close to zero (attend-in condition; Rayleigh test, FEF, $P < 0.001$, median = 7°, and V4, $P < 0.001$, median = –26°), corresponding to a time delay of 0.5 to 1.5 ms between spikes and the phase of maximum depolarization in the LFP at 50 Hz (Fig. 3A). By contrast, the phase of spike-field coherence across areas was shifted approximately half a gamma cycle [attend-in condition; Rayleigh test, FEF spikes–V4 LFPs, $P < 0.001$, median phase = –142° (or 218°), and V4 spikes–FEF LFPs, $P < 0.001$, median phase = 144° (or –216°)], corresponding to a time shift of ~8 (or 12) ms (Fig. 3A). Likewise, the median phase of spike-spike coherence pairs having a maximum gamma coherence peak of at least 0.1 was about 120°, which corresponds to a time shift of 7 ms. Similar results were found by com-

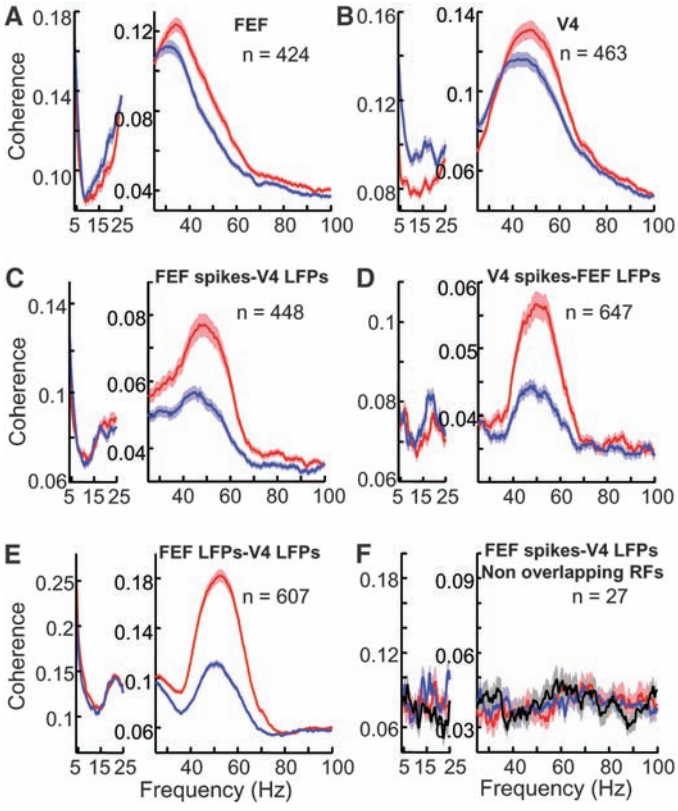

Fig. 2. Attentional enhancement of synchronization. (**A** to **D**) Spike-field coherence (A) within FEF, (B) within V4, (C) between spikes in FEF and LFPs in V4, and (D) between spikes in V4 and LFPs in FEF. (**E**) LFP-LFP coherence between FEF and V4 sites. Conventions are the same as in Fig. 1. (**F**) Spike-LFP coherence between FEF spikes and V4 LFPs from recording sites with nonoverlapping RFs (i) with attention inside the V4 RF during the post-stimulus period (red line), (ii) with attention in right hemifield, outside both V4 and FEF RFs during the post-stimulus period (blue line), and (iii) during the pre-stimulus period with no stimuli except for the fixation spot (black line). Tapers providing an effective smoothing of ±10 Hz were used for spectral estimation of higher frequencies [25 to 100 Hz, right part of (A) to (F)] and tapers providing smoothing of ±3 Hz were used for lower frequencies [<25 Hz, left part of (A) to (F)].

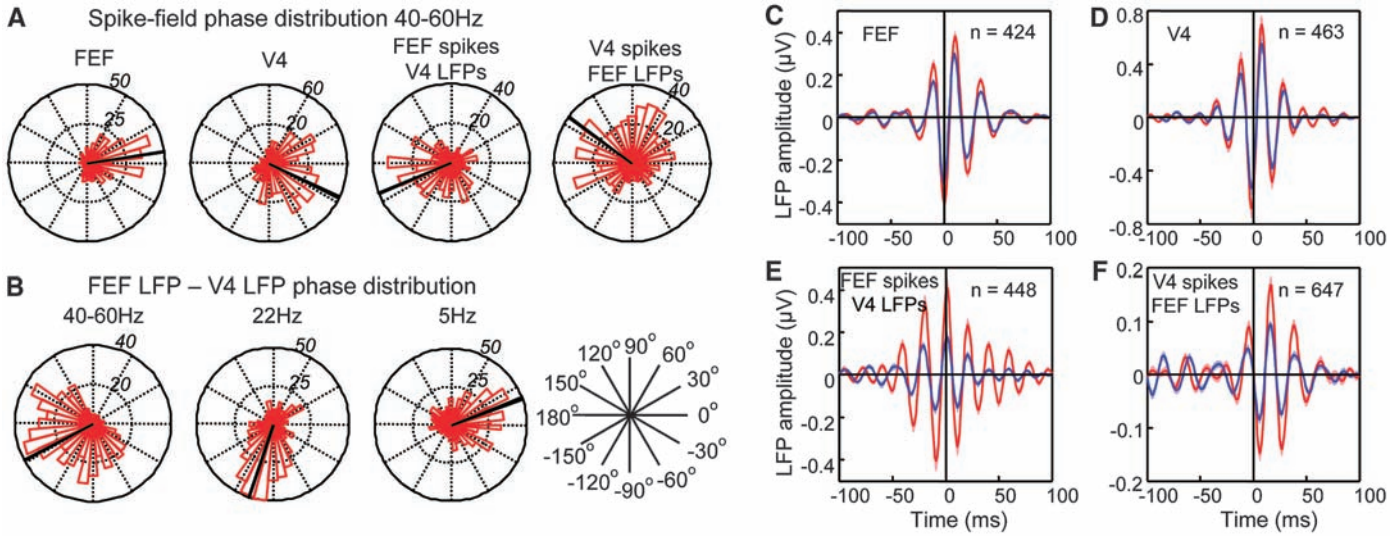

Fig. 3. Relative phase. (**A**) Distribution of average relative phase (40 to 60 Hz) between spikes and LFPs within and across areas. (**B**) Distribution of relative phases between FEF and V4 LFPs at different frequencies (40 to 60 Hz, 22 Hz, and 5 Hz). Shown are all phases from condition with attention inside the RF. (**C** to **F**) Spike-triggered averages of LFPs filtered between 35 and 80 Hz with (C) spikes and LFPs from FEF, (D) spikes and LFPs from V4, (E) spikes from FEF and LFPs from V4, and (F) spikes from V4 and LFPs from FEF. Conventions are the same as in Fig. 1.

paring spike-triggered averages of the LFP within and across areas (Fig. 3, C to F).

Although the peak coherence and largest attentional effects were in the gamma range, there was also coherence between FEF and V4 at other frequencies. We therefore tested whether the phase relationship at these other frequencies followed a fixed time shift of ~8 to 12 ms or a fixed phase shift of half a cycle. The medians of the distributions for the gamma, beta, and theta frequencies (40- to 60-Hz median = –152°, 22-Hz median = –105°, and 5-Hz median = 20°) correspond to time delays of –8, –13, and 11 ms, or a relatively fixed time shift of 8 to 13 ms in either direction rather than a fixed phase shift (Fig. 3B). A comparable (~10 ms) delay has been found between visual response latencies in anatomically connected areas along the ventral stream (*17*), suggesting that conduction times and synaptic delays account for the 8 to 13 ms shift in coupling.

The earlier latency of attentional effects on firing rates in FEF as compared with those in V4 suggests that FEF may initiate the coupled oscillations between the two areas. To further test this idea, we used Granger causality analysis to test the relative strength of influence of V4 on FEF LFPs and vice versa (*14*). Granger causality values for gamma increased with attention for both directions (paired t test, $P < 0.001$ for both directions) and were significantly above chance (FEF → V4 peak = 0.010 at 46 Hz and V4 → FEF peak = 0.025 at 55 Hz; permutation test, $P < 0.001$) (*14*), indicating that gamma activity in each area has a significant causal influence on the other area. However, the attentional effects on the Granger causality values appeared significantly earlier in the FEF-to-V4 direction than in the reverse direction (FEF to V4, 110 ms, and V4 to FEF, 160 ms; two-sided permutation test, $P < 0.05$) (Fig. 4, A and B), which is consistent with the idea that FEF initiates the gamma frequency oscillations in V4. The causality relationship reversed a short time later, with the Granger values becoming significantly larger in the V4-to-FEF direction around 300 ms after the cue onset (average 400 to 1000 ms after cue onset; paired t test, $P < 0.001$). In fact, the Granger values in the FEF-to-V4 direction greatly diminished across the trial.

We considered whether firing-rate changes with attention in FEF preceded the attentional effects on synchrony or vice versa. We used the Hilbert-Huang transform method (*18*) to calculate instantaneous LFP power over time in FEF and V4 (Fig. 4C). At the population level, significant attentional enhancement of gamma power in the LFP in FEF and V4 occurred at 120 ms and 100 ms, respectively (Fig. 4D), which was not a significant difference (two-sided permutation test, $P = 0.84$). To compare the relative latencies of attention effects on firing rate and LFP gamma power, we calculated the distribution of latencies for attentional effects across all individual sites in the first 300 ms after the cue onset. The distributions of attentional latencies in LFP gamma power in both FEF and V4 were significantly later than the distribution of latencies for attentional effects on firing rates in FEF (Wilcoxon rank-sum test, $P < 0.01$ for both comparisons) and significantly earlier than the distribution of latencies for attentional effects on V4 firing rates (Wilcoxon rank-sum test; V4 LFP gamma power, $P < 0.05$, and FEF LFP gamma power, $P < 0.001$) (table S2). Together, these results indicate that significant attentional effects on LFP gamma power in either area occur later than the earliest attentional effects on firing rates in the FEF. Rather than being caused by enhanced gamma oscillations, increases in firing rates in FEF with attention may initiate the coupled oscillations within and across areas. In contrast, firing-rate changes in area V4 occur later and might result at least in part from enhanced gamma oscillations.

In summary, the results suggest that FEF is a major source of the attentional effects on gamma frequency synchrony in V4 and probably other ventral stream areas. The Granger causality analyses suggest that top-down inputs from FEF to V4 predominate at the onset of spatially directed attention, but the bottom-up inputs from V4 to FEF come to predominate over the course of sustained attention. The coupled oscillations across areas are shifted in time by about 8 to 13 ms, which may be the optimal time shift to allow for spikes initiated in one area to affect cells at a peak depolarization phase in the coupled area (*17*). Tight coupling between the inputs and outputs of cells in V4 and FEF may also allow for enhanced spike timing–dependent plasticity of the connections between the two areas (*19*), which might mediate learning effects with attention. For distracting stimuli, or for sites with nonoverlapping RFs, these coupled oscillations are much smaller, which will reduce the impact of spikes in one area upon the other. We do not suggest that the attentional effects on gamma synchrony and firing rates in V4 are caused solely by inputs from FEF, because V4 receives inputs from several other structures that have been implicated in attention (*1*). However, these other inputs may also need to be synchronized at compatible frequencies and with the appropriate time shifts in order to support effective communication.

It has been suggested that low-frequency synchronization (for example, beta) is more suitable for long-range or polysynaptic communication across distant brain areas, with gamma rhythms being used for local computations (*20*). Although there is evidence for such low-frequency long-range synchronization (*21*–*25*), here we show that two distant but monosynaptically connected areas can be synchronized at gamma frequencies, which is probably not caused simply by common input (*21*). Enhanced oscillatory coupling has now been reported across several brain structures in monkeys (*4*, *23*, *26*) and other species (*21*, *24*, *27*) in association with attention and other behaviors, at a variety of frequencies, and may therefore be a general mechanism for regulating communication across brain structures (*6*, *28*).

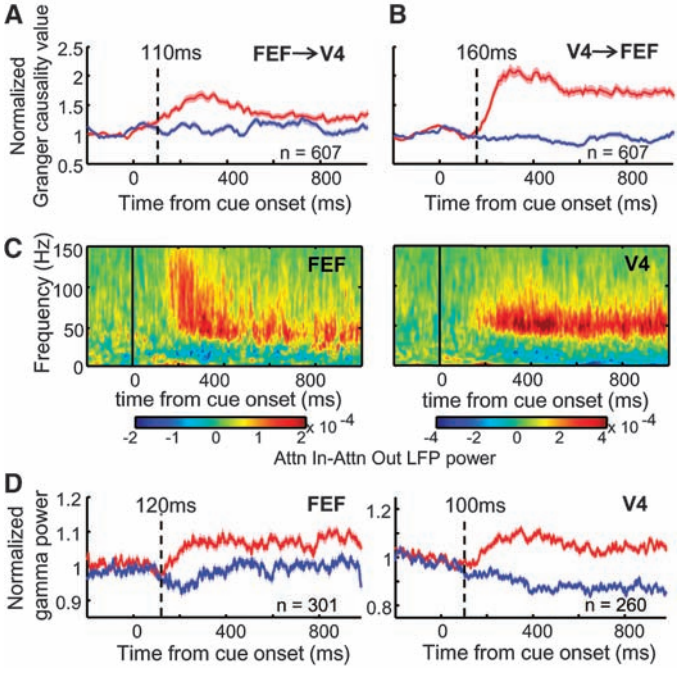

Fig. 4. Time-frequency synchrony measures and directional influences. (**A** and **B**) Population average of normalized Granger causality values averaged between 40 and 60 Hz across all pair-wise combinations of LFPs recorded in FEF and V4. Direction of influence is indicated by the arrows. (**C**) Population averages of attentional effects (attention inside RF–attention outside RF) on FEF and V4 power. (**D**) Normalized LFP gamma power in FEF and V4. Conventions are the same as in Fig. 1.

References and Notes

1. R. Desimone, J. Duncan, *Annu. Rev. Neurosci.* **18**, 193 (1995).
2. P. Fries, J. H. Reynolds, A. E. Rorie, R. Desimone, *Science* **291**, 1560 (2001).
3. N. P. Bichot, A. F. Rossi, R. Desimone, *Science* **308**, 529 (2005).
4. Y. B. Saalmann, I. N. Pigarev, T. R. Vidyasagar, *Science* **316**, 1612 (2007).
5. P. Lakatos, G. Karmos, A. D. Mehta, I. Ulbert, C. E. Schroeder, *Science* **320**, 110 (2008).
6. C. Borgers, S. Epstein, N. J. Kopell, *Proc. Natl. Acad. Sci. U.S.A.* **105**, 18023 (2008).
7. P. Tiesinga, J. M. Fellous, T. J. Sejnowski, *Nat. Rev. Neurosci.* **9**, 97 (2008).
8. E. K. Miller, J. D. Cohen, *Annu. Rev. Neurosci.* **24**, 167 (2001).
9. G. B. Stanton, C. J. Bruce, M. E. Goldberg, *J. Comp. Neurol.* **353**, 291 (1995).
10. J. D. Schall, A. Morel, D. J. King, J. Bullier, *J. Neurosci.* **15**, 4464 (1995).
11. L. G. Ungerleider, T. W. Galkin, R. Desimone, R. Gattass, *Cereb. Cortex* **18**, 477 (2008).

12. T. Moore, K. M. Armstrong, *Nature* **421**, 370 (2003).
13. L. B. Ekstrom, P. R. Roelfsema, J. T. Arsenault, G. Bonmassar, W. Vanduffel, *Science* **321**, 414 (2008).
14. Materials and methods are available as supporting material on *Science* Online.
15. P. Fries, T. Womelsdorf, R. Oostenveld, R. Desimone, *J. Neurosci.* **28**, 4823 (2008).
16. M. Zeitler, P. Fries, S. Gielen, *Neural Comput.* **18**, 2256 (2006).
17. L. G. Nowak, J. Bullier, in *Cerebral Cortex*, K. S. Rockland, J. H. Kaas, A. Peters, Eds. (Plenum, New York, 1997), vol. 12, pp. 205–241.
18. N. E. Huang *et al.*, *Proc. R. Soc. London Ser. A* **454**, 903 (1998).
19. Y. Dan, M. M. Poo, *Neuron* **44**, 23 (2004).
20. N. Kopell, G. B. Ermentrout, M. A. Whittington, R. D. Traub, *Proc. Natl. Acad. Sci. U.S.A.* **97**, 1867 (2000).
21. A. von Stein, C. Chiang, P. Konig, *Proc. Natl. Acad. Sci. U.S.A.* **97**, 14748 (2000).
22. A. Brovelli *et al.*, *Proc. Natl. Acad. Sci. U.S.A.* **101**, 9849 (2004).
23. B. Pesaran, M. J. Nelson, R. A. Andersen, *Nature* **453**, 406 (2008).
24. P. R. Roelfsema, A. K. Engel, P. Konig, W. Singer, *Nature* **385**, 157 (1997).
25. A. Sirota *et al.*, *Neuron* **60**, 683 (2008).
26. T. J. Buschman, E. K. Miller, *Science* **315**, 1860 (2007).
27. A. G. Siapas, E. V. Lubenov, M. A. Wilson, *Neuron* **46**, 141 (2005).
28. T. Womelsdorf, P. Fries, *Curr. Opin. Neurobiol.* **17**, 154 (2007).
29. We thank G. Pielli, D. Stock, and C. Alfes for help with the animal training and Z.-X. Liu for help with the Granger causality analysis. We also thank N. Bichot, R. Landman, G. Mulliken, and A. Mitz for helpful discussions. Supported by grants EY017292 and EY017921 to R.D. S.J.G. was supported in part by grant MH64445 from NIH (USA).

Supporting Online Material

www.sciencemag.org/cgi/content/full/324/5931/1207/DC1
Materials and Methods
SOM Text
Figs. S1 to S5
Table S1
References

26 January 2009; accepted 8 April 2009
10.1126/science.1171402

Genome-Wide Identification of Human RNA Editing Sites by Parallel DNA Capturing and Sequencing

Jin Billy Li,[1]* Erez Y. Levanon,[1]* Jung-Ki Yoon,[1]† John Aach,[1] Bin Xie,[2] Emily LeProust,[3] Kun Zhang,[1]‡ Yuan Gao,[2,4] George M. Church[1]§

Adenosine-to-inosine (A-to-I) RNA editing leads to transcriptome diversity and is important for normal brain function. To date, only a handful of functional sites have been identified in mammals. We developed an unbiased assay to screen more than 36,000 computationally predicted nonrepetitive A-to-I sites using massively parallel target capture and DNA sequencing. A comprehensive set of several hundred human RNA editing sites was detected by comparing genomic DNA with RNAs from seven tissues of a single individual. Specificity of our profiling was supported by observations of enrichment with known features of targets of adenosine deaminases acting on RNA (ADAR) and validation by means of capillary sequencing. This efficient approach greatly expands the repertoire of RNA editing targets and can be applied to studies involving RNA editing–related human diseases.

Adenosine-to-inosine (A-to-I) RNA editing converts a genomically encoded adenosine (A) into inosine (I), which in turn is read as guanosine (G), and increases transcriptomic diversity (*1*, *2*). It is critical for normal brain function (*3*–*7*) and is linked to various disorders (*8*). To date, a total of 13 edited genes have been identified within nonrepetitive regions of the human genome (table S1). The limiting factor in the identification of RNA editing targets has been the number of locations that could be profiled by the sequencing of DNA and RNA samples. Even with recent developments in massively parallel DNA sequencing technologies (*9*), it still remains expensive to sequence whole genomes and transcriptomes, both of which are required to identify RNA editing targets. Here, we report an efficient and unbiased genome-wide approach to identify RNA editing sites that uses tailored target capture followed by massively parallel DNA sequencing.

We first compiled a set of 59,437 genomic locations enriched with RNA editing sites, excluding repetitive regions such as *Alu* (fig. S1) (*10*). To reduce biases in detection, the key criteria for previous predictions of editing targets—conservation, coding potential, and RNA secondary structure (*11*–*15*)—were not taken into account. Over 90% of the previously identified editing targets are present in this data set (table S1). We designed padlock probes (*16*) for 36,208 sites that best satisfied our criteria for probe design (table S2) (*10*). Sites near splicing junctions required two different probes [targeting genomic DNA (gDNA) and cDNA], giving rise to a total of 41,046 probes designed for 36,208 sites (table S2).

To identify RNA editing sites, we used gDNA and cDNA from seven different tissues (cerebellum, frontal lobe, corpus callosum, diencephalon, small intestine, kidney, and adrenal), all derived from a single individual so as to rule out polymorphisms among populations. The pool of probes was hybridized to gDNA and cDNA in separate reactions (Fig. 1A and fig. S2). We sequenced the amplicons and identified sites where an A allele was observed in gDNA, whereas at least a fraction of G reads were present in the cDNA samples. A majority of sites were covered with multiple reads (Fig. 1B). Two independent

Table 1. Statistics of sequencing of samples used in this study.

Sample	Total reads	Mappable reads	Sites with ≥1 read	Fraction of sites with ≥1 read	RNA editing candidates*
gDNA (combined)	12,604,941	12,150,194	33,886	93.6%	N/A
Replicate 1	5,145,193	5,042,006	32,491	89.7%	N/A
Replicate 2	7,459,748	7,108,188	32,942	91.0%	N/A
cDNA					
Cerebellum	5,538,459	5,382,743	26,220	72.4%	126
Frontal lobe (combined)	14,065,388	13,360,868	28,382	78.4%	268
Replicate 1	6,950,660	6,563,630	26,617	73.5%	238
Replicate 2	7,114,728	6,797,238	26,628	73.5%	230
Corpus callosum	5,096,832	4,963,983	25,447	70.3%	180
Diencephalon	5,420,151	5,291,184	25,187	69.6%	172
Small intestine	6,516,258	6,172,901	26,845	74.1%	181
Kidney	6,354,025	5,984,709	26,299	72.6%	177
Adrenal	2,251,755	2,188,637	23,589	65.1%	121

*A site with evidence for RNA editing is required to have an editing level of ≥5% and a log-likelihood (LL) score of ≥2 (*10*).

[1]Department of Genetics, Harvard Medical School, 77 Avenue Louis Pasteur, Boston, MA 02115, USA. [2]Center for the Study of Biological Complexity, Virginia Commonwealth University, 1000 West Cary Street, Richmond, VA 23284, USA. [3]Genomics Solution Unit, Agilent Technologies, 5301 Stevens Creek Boulevard, Santa Clara, CA 95051, USA. [4]Department of Computer Science, Virginia Commonwealth University, 401 West Main Street, Richmond, VA 23284, USA.

*These authors contributed equally to this work.
†Present address: College of Medicine, Seoul National University, Seoul 110-799, Korea.
‡Present address: Department of Bioengineering, University of California, San Diego, CA 92093, USA.
§To whom correspondence should be addressed. E-mail: http://arep.med.harvard.edu/gmc/email.html